Published in final edited form as:
Energy Sustain Soc. 2013 September 1; 6(9): 2706–2713. doi:10.1039/C3EE41321G.

A H_2-evolving photocathode based on direct sensitization of MoS3 with an organic photovoltaic cell

Tiphaine Bourgeteau[a], **Denis Tondelier**[b], **Bernard Geffroy**[a,b], **Romain Brisse**[a], **Christel Laberty-Robert**[c], **Stéphane Campidelli**[a], **Rémi de Bettignies**[d], **Vincent Artero**[e], **Serge Palacin**[a], and **Bruno Jousselme**[a,*]

[a]CEA-Saclay, DSM/IRAMIS/SPCSI/Laboratoire de Chimie des Surfaces et Interfaces, 91191 Gif sur Yvette Cedex, France

[b]Laboratoire de Physique des Interfaces et Couches Minces, Ecole Polytechnique, CNRS, 91128 Palaiseau, France

[c]Laboratoire de Chimie de la Matière Condensée de Paris-UMR 7574, Université Paris 6, Collège de France, 11 place Marcelin Berthelot 75005, Paris, France

[d]INES, CEA-DRT/LITEN/DTS/LMPV, Institut National de l'Energie Solaire, Le Bourget du Lac, France

[e]Laboratoire de Chimie et Biologie des Métaux, Université Grenoble 1, CNRS, CEA, 17 rue des Martyrs 38054, Grenoble Cedex 9, France

Abstract

An organic solar cell based on a poly-3-hexylthiophene (P3HT): phenyl-C_{61}-butyric acid (PCBM) bulk hetero-junction was directly coupled with molybdenum sulfide resulting in the design of a new type of photocathode for the production of hydrogen. Both the light-harvesting system and the catalyst were deposited by low-cost solution-processed methods, i.e. spin coating and spray coating respectively. Spray-coated MoS_3 films are catalytically active in strongly acidic aqueous solutions with the best efficiencies for thicknesses of 40 to 90 nm. The photocathodes display photocurrents higher than reference samples, without catalyst or without coupling with a solar cell. Analysis by gas chromatography confirms the light-induced hydrogen evolution. The addition of titanium dioxide in the MoS_3 film enhances electron transport and collection within thick films and therefore the performance of the photocathode.

1. Introduction

Providing energy for our planet in a sustainable way is one of the biggest challenges of this century. Among renewable sources of energy, sunlight is by far the most exploitable one, being inexpensive, non-polluting and abundant. Yet efficient harvesting, conversion and storage of solar energy remain a major challenge for smoothing out the temporal fluctuations of solar power and allowing on-demand use.[1] Solar to chemical energy conversion, i.e. production of a fuel that carries a high energetic density stored within chemical bonds, is

*Fax: +33 169086462, Tel: +33 169089191 ; bruno.jousselme@cea.fr.

†Electronic Supplementary Information (ESI) available: TEM images and EDX spectrum of MoS_3 nanoparticles (Fig. S1 and S2). MoS_3 films characterizations (Fig. S3, profilometry; Fig. S4, SEM; Fig. S5 to S7, CVs; Fig. S8, Impedance; Fig. S9 to S11, XPS). Mixed TiO_2:MoS_3 films characterizations (Fig. S12, CVs; Fig. S13, Impedance). Photocathode characterizations (Fig. S14, electrolysis; Fig. S15, gas chromatography). Current-voltage curves of P3HT:PCBM solar cells (Fig. S16). See DOI: 10.1039/b000000x/

Europe PMC Funders Author Manuscripts

very promising.[2-8] In particular, hydrogen produced through water splitting has emerged as a potential fuel for sustainable energy cycles, because its oxidation 'back' to water in a fuel-cell efficiently restitutes the stored energy, in the form of electricity and without waste.[3, 5] Up to now, solar hydrogen generation is efficient only in systems that use expensive photovoltaic cells to power electrolysis.[9] Direct and low cost production of hydrogen from sunlight and water would be an ideal long-term solution, but is still a challenging issue.[2, 9-11]

To that aim, photoelectrochemical (PEC) cells have been developed.[1, 12] These devices combine two photoelectrodes achieving the oxygen evolution reaction (OER, i.e. oxidation of water into oxygen) and the hydrogen evolution reaction (HER, i.e. reduction of water into hydrogen).[13] Most of the PEC cells developed so far rely on highly efficient multicomposite photovoltaic modules, with high processing costs, long energetic pay-back and containing rare/toxic elements.[13-16] Remarkable exceptions exploit low-cost molecular dyes for light harvesting in dye-sensitized solar cells (DSSCs): the tandem cells developed by Grätzel[17] or by Dismukes and Spiccia[18, 19] combine cheap metal (Fe, W, Mn) oxides as oxygen-evolving photocatalysts and dye-sensitized TiO_2-based photoanodes.

Besides DSSCs, molecular-based photosensitizers are used for the construction of organic photovoltaic (OPV) cells. Organic photovoltaics hold promises for the development of solar cells,[20-22] with conversion efficiencies having recently reached more than 10 %.[23, 24] Low-cost and lightweight materials processed at lower temperatures account for the main advantages of OPVs in terms of environmental sustainability and economic viability.[25] This technology has been scarcely used in the context of hydrogen evolution, once with the photoactive layer in direct contact with the electrolyte for the construction of a PEC cell, [26] or recently in a wired configuration with a triple-junction OPV cell powering a water electrolyzer.[27]

We report here how the well-known poly-3-hexylthiophene : phenyl-C_{61}-butyric acid bulk heterojunction (P3HT:PCBM) can be used for promoting light-driven hydrogen evolution. Instead of platinum, undoubtedly the best catalyst for HER but scarce and expensive,[28-30] we selected molybdenum sulfides (MoS_x)[29, 31-38] among other recently developed noble metal-free, earth-abundant HER catalysts.[12, 39-41] These promising catalytic materials are indeed able to operate in water. We thus undertook the coupling of the P3HT:PCBM active layer with a catalytic layer of MoS_3 as shown in Figure 1 and investigated the performances of the resulting H_2-evolving photocathode under acidic aqueous conditions.

2. Results and discussion

2.1. Synthesis and characterization of amorphous MoS_3 particles

Crystalline MoS_2 nanoparticles were the first molybdenum sulfide catalysts with HER properties to be developed. They were originally synthesized by physical vapor deposition at high temperature using Mo and H_2S,[32] or by dry impregnation of $(NH_4)_6Mo_7O_{24}$ or $(NH_4)_2[MoS_4]$ followed by high temperature treatment in H_2S and H_2.[42] Soft low-temperature methods such as electrochemistry,[35] precipitation[36] and exfoliation[38] were recently developed to generate catalytically active amorphous MoS_2 or MoS_3. Precipitation seems to be the most convenient method to cast pre-formed catalytic nanoparticles on the active P3HT:PCBM layer. We thus synthesized MoS_3 particles by addition of aqueous HCl to an aqueous suspension of MoO_3 and Na_2S, according to the method of Hu and coll.[36] To investigate the influence of the pH of the solution on the structure and composition of the particles, three batches were prepared with distinct final pHs (2.0, 2.7 and 3.5). The particles were then separated by centrifugation, washed several times with deionized water, and

dispersed in acetone to a concentration of 6 $g.L^{-1}$. Separation by centrifugation was easier for low final pHs, indicating that pH influences the aggregation of particles.

TEM analysis (Fig. 2 and S1) was performed for each synthesized batch and showed isolated particles with 4 Å diameter and short chains of particles in the form of rods with 1-2 nm length. While an aggregation process eases the separation of the particles from the reaction mixture when the pH goes from 3.5 to 2, the final pH has no influence on the individual particle size. EDX analysis (Fig. S2) only shows molybdenum and sulfur, as well as residual traces of elements such as sodium and oxygen present in the starting materials, and carbon coming from atmospheric contamination.

2.2. Fabrication and electrocatalytic properties of MoS_3-coated electrodes

Electrodes were fabricated by spin coating or spray casting of the suspension of MoS_3 on ITO-coated glass substrates. MoS_3 films with controlled and tunable thickness are obtained with spin coating of concentrated suspensions of MoS_3 diluted with acetone on ITO-coated substrates. The thickness of the resulting films was evaluated by profilometry and found proportional to the amount of MoS_3 in the spin-coated suspension (Fig. S3). Very thin films (~ 5 nm) can be obtained from diluted solutions (1 $g.L^{-1}$). This method allows for the reproducible deposition of smooth and homogeneous films as shown by SEM measurements (Fig. S4a). By comparison, spray cast of MoS_3 suspensions in acetone yields rough and non-homogeneous films in our conditions (Fig. S4b). The thicknesses of spray-cast films are therefore given with large error bars and it was not possible to get films with thickness under 15 nm.

The catalytic activity of the electrode towards HER was studied by cyclic voltammetry at 50 $mV.s^{-1}$ in aqueous H_2SO_4 solutions. The catalytic layer showed high activity for HER at pH 0 (0.5 M H_2SO_4), with an onset overpotential of 180 mV (Fig. 3) as previously described.[36] Higher onset overpotentials are measured for less acidic conditions. We note that the catalytic current is proportional to the proton concentration (Fig. S5). Production of hydrogen was confirmed by gas chromatography measurements. The particles synthesized at different pH displayed similar catalytic current and onset potential (Fig. S6). It is worth to note that no catalytic activity was observed on bare ITO electrodes under the same conditions.

The influence of the thickness of the MoS_3 films on the catalytic activity was then investigated (Fig. 3). We first describe the results obtained on spin-coated samples for which reproducible and homogeneous thicknesses are obtained. Low HER activity are observed for thick (>200 nm) films. The conductivity of molybdenum sulfide is known to be low (10^{-5} $S.cm^{-1}$).[43] We thus assigned this behavior to the large resistivity of these coatings, preventing electron transport to the surface for catalytic reduction of protons. Thinner films display better catalytic currents but very thin films (<15 nm) are less efficient, probably because of a reduced active surface area. These films actually showed poor stability under working conditions compared to thicker films and their activity drops by 50% after electrolysis at −0.6 V vs. Ag/AgCl for 1h. The decrease of MoS_3 performances due to catalyst release for very thin films can be visually assessed by the reduced color intensity of the film. Films with thicknesses between 40 and 90 nm show optimal current densities and onset potentials, together with good stability during electrolysis: the drop in current density is limited to 30% after electrolysis.

The same behavior is observed for spray-cast films (Fig. 4). Sprayed MoS_3 films show the same electrocatalytic properties as spin coated films, though the current densities are lower, e.g. by 20% for a 30 nm film (Fig. S7). Figure 4 compares the electrocatalytic performances of three sprayed films with distinct thicknesses. High thickness results in increased onset

overpotentials and lower current densities. Again, optimal catalytic performances are obtained for films with thickness between 40 and 100 nm. Impedance spectra were recorded for these three sprayed samples at −0.19 V vs. RHE (close to the onset potential) in 0.5 M H_2SO_4 (Fig. S8). Calculated charge transfer resistances are 60 $\Omega.cm^2$ (40 ± 20 nm), 110 $\Omega.cm^2$ (100 ± 30 nm) and 378 $\Omega.cm^2$ (300 ± 100 nm) respectively: they are increasing with the thickness of the layer, corroborating the conclusions drawn from cyclic voltammetry experiments.

XPS analysis was carried out on spin-coated MoS_3 films, before and after a cyclic voltammetry (CV) experiment. The XPS survey spectra (Fig. S9) shows peaks due to molybdenum and sulfur, as well as some impurities such as sodium and oxygen (present in the precursors used for the synthesis), and carbon (atmospheric contamination). Mo3d spectra before (after) CV (Fig. S10) show binding energies of $Mo3d_{5/2}$ and $Mo3d_{3/2}$, at 228.9 eV (229.0 eV) and 232.1 eV (232.2 eV) respectively. These signals correspond to Mo in the +IV oxidation state, as previously reported.[30, 36] Mo^{VI} from residual MoO_3 starting material is also observed at 231.9 and 235.0 eV (before CV) and 231.8 and 234.7 eV (after CV). Analysis of the S_{2p} region before (after) CV (Fig. S11) reveals two types of sulfur atoms: peaks at 161.2 (161.3) and 162.7 (162.3) eV are assigned to $S2p_{3/2}$ and $S2p_{1/2}$ signals of sulfide (S^{2-}) anions while peaks at 162.5 (162.8) and 163.8 (163.8) eV correspond to $S2p_{3/2}$ and $S2p_{1/2}$ signals of disulfide (S_2^{2-}) anions. Quantification based on S2p and Mo3d areas using Wagner coefficients shows an initial S:Mo ratio of 2.85. The MoS_3 structure has been widely discussed since the first studies by Ratnasamy and coll.[44] Two main structures have been considered: a-MoS_3 consisting of disordered chains[45] and MoS_3 built from Mo_3 triangles.[46] Hibble and coll. showed that the chain model and the formula $Mo^{IV}(S^{2-})(S_2^{2-})$ fits well with the experimental results.[45] The isolated particles of ~4 Å diameter observed in TEM (Fig. 2) could correspond to triangular Mo_3 clusters surrounded by sulfur atoms[46] knowing that Mo-Mo distances lie in the observed range (≈ 2.7 Å and ≈ 3.7 Å)[47] while the 1-2 nm long rods better fit with the chain model. After CV, the area of Mo^{IV} and Mo^{VI} signals both decreased, indicating that Mo is released in aqueous media which may be the reason for the observed decrease in activity.[37] In the same time, the sulfide to disulfide ratio increases from 1.1 to 2.1 and the S:Mo ratio varies from 2.9 to 2.1. All these observations indicate that the composition in the film evolves during CV as previously reported with transformation of a MoS_3 phase into a MoS_x (x > 2) phase.[36]

2.3. Fabrication and characterization of mixed TiO_2:MoS_3 electrodes

The P3HT:PCBM layer is sensitive to oxygen and above all to water, as demonstrated recently.[48, 49] Therefore, a thick catalytic layer has to be used for the construction of the targeted photocathode in order to protect the organic solar cell. However, due to the high resistivity of MoS_3, a low catalytic HER activity is obtained for thick films. In addition, the coating of the OPV layer favors recombination inside the light-harvesting material. In bulk-heterojunction polymer solar cells, densely packed n-type oxide TiO_2 is often placed between the light-harvesting active layer and the charge-collecting electrode.[50, 51] This interfacial material improves the performances of the solar cell[20] because of its good electron transport properties. The long-term stability is also enhanced since TiO_2 prevents direct contact between oxygen and water and the active layer.[50, 52, 53] In addition this large band-gap semi-conductor is transparent to visible light and thus does not compete with the light-harvesting layer. We thus decided to mix our MoS_3 material with commercially available TiO_2 particles. As for MoS_3, mixed MoS_3:TiO_2 suspensions (v/v = 1/1) have been deposited by spin coating to study the influence of the thickness, and spray casting as used for the deposition on OPV cells.

Cyclic voltammograms were measured at 50 $mV.s^{-1}$ in H_2SO_4 0.5 M for mixed TiO_2:MoS_3 (approximate mass ratio: 5:1) coated electrodes (Fig. S12). The overpotential for hydrogen

evolution is similar to MoS_3 alone. Mixed TiO_2:MoS_3 electrodes (100 ± 20 nm thickness) display similar onset potential and catalytic HER current to MoS_3 (20 nm thickness) alone.

Impedance measurements (Fig. S13) confirmed that the charge transfer resistance of the mixed TiO_2:MoS_3 (approximate mass ratio 5:1, 20 Ω.cm^2) is decreased by 170 Ω.cm^2 compared to MoS_3 (190 Ω.cm^2). Therefore, it seems that TiO_2, besides acting as a good electron contact for electrons generated by the OPV layer, also improves the charge transfer from ITO to MoS_3 thanks to its good electron photoconductivity.[54]

2.4. Fabrication and photoelectrocatalytic properties of MoS_3/OPV photocathodes

With the above know-how for fabrication of MoS_3-based catalytic layer, we undertook the fabrication of photocathodes as shown in Figure 1 based on a bulk heterojunction between two organic semi-conductors. We choose the popular P3HT:PCBM mixture because it allows for the construction of OPV cells with an average efficiency of 3.5%,[55] which was sufficient for this proof-of-concept study. We successively deposited a hole-transporting layer (PEDOT:PSS), an active layer (P3HT:PCBM) and a catalytic layer (MoS_3 or mixed TiO_2:MoS_3) on ITO-coated glass substrates. Our primary goal was to deposit each layer by spin-coating. This was possible for both the PEDOT:PSS and P3HT:PCBM layers for which we obtain films with 40 nm and 150 nm thickness respectively. However, even with surfactants such as Brij®, we could not spin-coat the catalytic layer on the P3HT:PCBM layer, since neither the suspension of MoS_3 nor that of mixed TiO_2:MoS_3 correctly wets the P3HT:PCBM layer. We therefore turn to spray-casting on the heated substrate to coat the active layer with the catalyst. It is worth to note that each layer was deposited from solutions by processes that can be easily scaled up to industrial processes such as roll-to-roll printing and spray-coating. Thicknesses of catalytic layers on P3HT:PCBM were difficult to evaluate because of the soft nature of P3HT:PCBM. Same conditions (time and concentrations) as previously developed were however used.

Two distinct photocathodes were prepared: one containing a catalytic layer based on MoS_3 and a second one with a thicker mixed TiO_2:MoS_3 catalytic layer. In order to discriminate between the effects of MoS_3 and TiO_2 on the performances, we also prepared two reference photoelectrodes, one without catalytic layer and another one only with a TiO_2 layer.

We then investigated the photoelectrocatalytic performances of the two photocathodes containing either MoS_3 or mixed TiO_2:MoS_3 as catalytic layer. The photocathodes were interfaced with a 0.5 M H_2SO_4 aqueous solution as shown in Figure 1 and irradiated with visible light from a Xe lamp filtered from UV and IR radiation. Figure 5 shows the photocurrents obtained for both photocathodes at an applied potential of −0.05 V vs. Ag/AgCl (0.16 V vs. RHE). The photocurrent obtained for the MoS_3/P3HT:PCBM photocathode (30 μA.cm^{-2}, blue trace) is only slightly higher than the one measured for the same stack but lacking the catalyst layer used as a reference (25 μA.cm^{-2}, black trace). By contrast, the photocathode based on the mixed TiO_2:MoS_3 catalytic layer yields a significantly higher photocurrent (>100 μA.cm^{-2}, red trace), highlighting the role of TiO_2 for promoting catalysis in this photocathode design.

Linear sweep voltammetry measurements were carried out at 5 mV.s^{-1} from 0.55 to −0.4 V vs. RHE, under chopped visible light (Fig. 6). The photocurrent of the reference photocathode without catalytic layer barely increases when the applied potential was swept to negative potentials. Solar-to-chemical energy storage implies that the chemical reaction is performed with a lower energy input as compared to the reaction in the dark. In that case, this implies that the electrochemical potential (the bias) is more positive than the thermodynamic potential of the H^+/ H_2 couple under the given conditions. The photocurrent displayed by the MoS_3 / P3HT:PCBM stack significantly differs from the reference

photocathode only for potentials more negative than 0 V vs. RHE, which corresponds to the thermodynamic potential for H_2 evolution at pH 0.2. This photocathode thus does not allow for energy storage. By contrast, the TiO_2 / P3HT:PCBM photocathode displays photocurrents with onset potential of ~0.5 V vs. RHE, confirming the ability for TiO_2 to efficiently extract charges from the OPV layer and to transfer them to the interface with the electrolyte. However, the photocurrent value plateaus at 100 $\mu A.cm^{-2}$ while the TiO_2:MoS_3/ P3HT:PCBM photocathode presents increased photocurrent values (200 $\mu A.cm^{-2}$ at 0 V vs. RHE and up to 300 $\mu A.cm^{-2}$ at −0.4 V vs. RHE).

Electrolyses at +0.16 V vs. RHE were carried out for 45 min to study the stability of the devices (Fig. S14). The photocurrent of the TiO_2:MoS_3 / P3HT:PCBM photocathode decreased by 30 % along that time. Hydrogen production was confirmed by gas chromatography (Fig. S15) during this experiment and the faradic yield was found similar to that determined for the catalytic layer under similar but purely electrocatalytic dark conditions. By contrast the photocurrent of the MoS_3 / P3HT:PCBM photocathode decreased by 50%. These data clearly show that TiO_2 protects the underlying organic photovoltaic component during continuous photocatalysis but that this component is unable to sustain H_2 evolution in the absence of a proper catalyst such as MoS_3.

The above results demonstrate the possibility to exploit OPV technology for the construction of a novel type of PEC devices harvesting visible light, though devices would need to operate efficiently (>80%) for years to be economically viable. The photocurrent values are still below those reported for photocathodes based on p-type silicon[34, 56-60] or Cu_2O[61] but the onset potential measured under irradiation is more positive by several hundreds of millivolts and gets close to that recently reported for the novel p-type WSe_2 material,[62] thus allowing for true energy storage. Our construction nevertheless display HER photocurrents significantly higher than those reported for photocathodes based on other solid-state semi-conductors, such as indium phosphide nanocrystals,[30] or dye-sensitized TiO_2 electrodes.[63, 64]

MoS_x is currently becoming a very popular HER catalytic material[33] and this material has been used for the design of various H_2-evolving nanoparticulate systems[37, 65-68] or Si-based photocathodes.[58, 59] In the present case, the catalytic layer has to be deposited on a molecular-based light-harvesting layer and a key issue consists in correctly interfacing the H_2-evolving catalyst with the donor material of the bulk heterojunction. Actually TiO_2 seems quite efficient in that respect and our optimal stack displays onset potential for light-driven H_2 production ~600 mV more positive than the onset HER potential measured at a TiO_2:MoS_3 electrode in the dark (Fig. 4). This photo-potential nicely matches the 570 mV open-circuit potential (V_{OC}) measured for 4.1 % efficiency solar cells based on the same P3HT:PCBM light-harvesting layer and produced in our laboratory under similar conditions (Fig. S16). The current density, however, remains lower than expected since the same solar cell can deliver a short circuit intensity of 11.3 $mA.cm^{-2}$. Clearly such high intensities are not sustained by the catalyst unless very cathodic potentials are applied but, from Fig. 4, current densities of the milli-ampere magnitude are attainable. Thus, further optimization is a serious challenge that seems possible based on the improvement of the interfacial layer, which should extract electrons from the OPV layer and convey them to the catalyst, while protecting the OPV core. Actually, deposition by sputtering of an 100 nm aluminum layer between the P3HT:PCBM and the TiO_2: MoS_3 layers resulted in 5-fold increased photocurrents. The preliminary results demonstrate that addition of an electron-collecting layer, aluminum, improves the overall performances of the photocathode. But aluminum, routinely used in OPV technology,[20] does not withstand the highly acidic conditions used here; we will report later on our effort to overcome these issues.

3. Conclusions

The combination of MoS_3 nanoparticles as a H_2-evolving catalyst with the core of an organic photovoltaic cell yields a novel type of photoelectrode achieving the reductive half reaction involved in water splitting. This system is based on earth-abundant elements and can be easily processed using low cost and low temperature spin-coating and spray-casting methods. Photoelectrochemical performances could be improved through the optimization of the thickness of the catalytic MoS_3 layer and its combination with TiO_2 so as to optimize electron transport at the interface between the light-harvesting and charge generating core and the catalytic layer. These promising results open novel avenues for the design of PEC devices with improved performances given the high number of parameters that are still prone to optimization, i.e. the nature, thickness and structuration of the core organic solar cell materials, the interfacial layer and catalyst. In particular the use of metal-doped MoS_2 materials[69, 70] or bioinspired catalysts[28, 71, 72] allowing to work under less acidic conditions is a promising research direction.

4. Experimental

4.1. Methods of characterization

Transmission Electronic Microscopy and Energy-dispersive analyses were carried out with a TECNAI 120 Spirit G2 from FEI and a CCD camera on column bottom Orius from Gatan in 4K steps. XPS data were collected by an Axis Ultra DLD (Kratos Analytical) using a monochromatic Al Kα X-ray source (1486.6 eV). The samples were illuminated with a 300 W xenon lamp (Oriel, ozone free) operated at 280 W coupled with a water-filled Spectra-Physics 6123NS liquid and a Spectra-Physics 59472 UV cut-off filter (λ >400 nm). Electrochemical measurements were recorded by a BioLogic Model VSP 0254. The thickness of the films was determined using Ambios XP-200 profilometer. More detailed methods are provided in the SI.

4.2. Chemicals and reagents

All manipulations were carried out under an inert Ar atmosphere using glovebox techniques unless otherwise mentioned. PEDOT:PSS (AI 4083 for spin coated devices) and the suspension of TiO_2 (Ti-Nanoxide HT-L/SC) were purchased from Ossila and Solaronix respectively. P3HT (M101, RR = 96.6 %) and P60CBM (M111, 99.0 % purity) were purchased from Ossila. Unless noted, all other reagents were purchased from commercial sources and used without further purification. ITO-coated glass substrates (XY20s) were purchased from Xinyan Technology Ltd.

4.3. Synthesis of MoS_3 nanoparticles

MoS_3 particles were synthesized according to a procedure from Merki et al.[36] In a typical preparation, molybdenum trioxide (0.51 g, 3.48 mmol) was added to an aqueous solution of sodium sulfide (1.34 g, 17.37 mmol of anhydrous Na_2S in 125 mL of water) to form a bright yellow solution. This solution was then kept under vigorous stirring while 6.0 M aqueous HCl was added slowly (10 minutes) until the pH was under 4. Three batches were synthesized, ending at pH 2, 2.7 and 3.5 respectively. At first, darkening of the solution was observed. After the addition of acid, the solution was boiled for 30 minutes, resulting in an increase of the pH by 1 unit. After being cooled to ambient temperature and instead of separating and washing the particles by vacuum filtration, the suspension was centrifuged, the supernatant liquid was thrown away and particles were dispersed in DI water. This process was repeated twice to wash the particles. The last precipitate was dispersed in acetone. The suspension was then sonicated for 5 minutes using an ultrasonic horn at 20 kHz.

4.4. Deposition of the MoS_3 nanoparticles

On ITO/glass substrate—MoS_3 films were sprayed (Aztek A470 airbrush with a 9344C nozzle) onto heated (100°C) ITO-coated glass substrates, cleaned by ultrasound bath in acetone for 15 min followed by 15 min in UV-ozone cleaner, from suspensions of MoS_3 in acetone. The thickness was evaluated by profilometry.

MoS_3 films were spin coated (Laurell Technologies Corporation device, model WS-400B-6NPP/LITE/OND) onto ITO-coated glass substrates, cleaned by ultrasound bath in acetone for 15 min followed by 15 min in UV-ozone cleaner, from suspensions of MoS3 (1.2 $g.L^{-1}$; 1.9 $g.L^{-1}$; 6 $g.L^{-1}$; 16 $g.L^{-1}$) diluted with acetone. Spin coating was performed in air by spinning at 2,000 rpm for 60s (ramp 5s).

A suspension (1 mL) of TiO_2 (8-10 nm nanocrystalline particles, 3% wt.) was mixed with 1 mL of a suspension of MoS_3 (6 $g.L^{-1}$, or diluted and deposited by spray casting or spin coating for characterization. By spin coating at 2000 rpm for 60s, a 100 nm–thick layer was obtained. By spray casting, the thickness was evaluated by profilometry.

Fabrication of the MoS_3-coated organic solar cell (MoS_3/OPV)—The organic solar cell was entirely solution-processed, in a glove box under argon atmosphere. On the ITO-coated glass substrate, cleaned by ultrasound bath in acetone for 15 min followed by 15 min in UV-ozone cleaner, PEDOT:PSS was filtered with a PVDF filter and spin coated (ramp 5s to 3000rpm, 45s at 3000rpm, then ramp 5s to 3500rpm, and 45s at 3500rpm). After thermal treatment for a few minutes at 130°C, P3HT:PCBM blend was also filtered with a 0.45 μm polypro filter and spin-coated on the top of the PEDOT:PSS layer (ramp 5s to 1500rpm, 40s at 1500rpm). The P3HT to PCBM ratio was 1 to 1, with [P3HT] = 15 $g.L^{-1}$ in ortho-dichlorobenzene. Before spin coating, the solution was stirred overnight at room temperature. Then, the MoS_3 catalytic layer, with or without TiO_2, was spray-cast on top of the heated (100°C) solar cell in the air, and quickly retransferred into the glove box for sintering at 120°C for 30min.

Supplementary Material

Refer to Web version on PubMed Central for supplementary material.

Acknowledgments

We are indebted to the CEA for the financial support, through the DSM Energie Program for the Ph. D thesis grant assigned to RB, the French National Research Agency (ANR, Labex program ARCANE, 11–LABX–003) and the European Research Council under the European Union's Seventh Framework Programme (FP/2007-2013)/ERC Grant Agreement n.306398). We also thank P. Le Griel and J. Fize for their assistances in the TEM characterizations and chromatographic measurements (H_2 quantification), respectively.

Notes and references

1. Walter MG, Warren EL, McKone JR, Boettcher SW, Mi Q, Santori EA, Lewis NS. Chem. Rev. 2010; 110:6446–6473. [PubMed: 21062097]
2. Lewis NS, Nocera DG. PNAS. 2006; 103:15729–15735. [PubMed: 17043226]
3. Esswein AJ, Nocera DG. Chem. Rev. 2007; 107:4022–4047. [PubMed: 17927155]
4. Cook TR, Dogutan DK, Reece SY, Surendranath Y, Teets TS, Nocera DG. Chem. Rev. 2010; 110:6474–6502. [PubMed: 21062098]
5. Turner JA. Science. 2004; 305:972–974. [PubMed: 15310892]
6. Thapper A, Styring S, Saracco G, Rutherford AW, Robert B, Magnuson A, Lubitz W, Llobet A, Kurz P, Holzwarth A, Fiechter S, de Groot H, Campagna S, Braun A, Bercegol H, Artero V. Green. 2013; 3:43.

7. Faunce T, Styring S, Wasielewski MR, Brudvig GW, Rutherford AW, Messinger J, Lee AF, Hill CL, deGroot H, Fontecave M, MacFarlane DR, Hankamer B, Nocera DG, Tiede DM, Dau H, Hillier W, Wang L, Amal R. Energy Environ. Sci. 2013; 6:1074–1076.
8. Faunce TA, Lubitz W, Rutherford AW, MacFarlane D, Moore GF, Yang P, Nocera DG, Moore TA, Gregory DH, Fukuzumi S, Yoon KB, Armstrong FA, Wasielewski MR, Styring S. Energy Environ. Sci. 2013; 6:695–698.
9. Turner JA. Science. 1999; 285:687–689. [PubMed: 10426982]
10. Grätzel M. Nature. 2001; 414:338–344. [PubMed: 11713540]
11. Lewis NS. Science. 2007; 315:798–801. [PubMed: 17289986]
12. Tran PD, Wong LH, Barber J, Loo JSC. Energy Environ. Sci. 2012; 5:5902–5918.
13. Khaselev O, Turner JA. Science. 1998; 280:425–427. [PubMed: 9545218]
14. Nocera DG. Acc. Chem. Res. 2012; 45:767–776. [PubMed: 22475039]
15. Yamada Y, Matsuki N, Ohmori T, Mametsuka H, Kondo M, Matsuda A, Suzuki E. Int. J. Hydrogen Energy. 2003; 28:1167–1169.
16. Rocheleau RE, Miller EL, Misra A. Energy Fuels. 1998; 12:3–10.
17. Grätzel M. CaTTech. 1999; 3:4–17.
18. Brimblecombe R, Koo A, Dismukes GC, Swiegers GF, Spiccia L. J. Am. Chem. Soc. 2010; 132:2892–2894. [PubMed: 20155923]
19. Hocking RK, Brimblecombe R, Chang L-Y, Singh A, Cheah MH, Glover C, Casey WH, Spiccia L. Nat. Chem. 2011; 3:461–466. [PubMed: 21602861]
20. Yip H-L, Jen AKY. Energy Environ. Sci. 2012; 5:5994–6011.
21. Kippelen B, Bredas JL. Energy Environ. Sci. 2009; 2:251–261.
22. Espinosa N, Hosel M, Angmo D, Krebs FC. Energy Environ. Sci. 2012; 5:5117–5132.
23. You J, Dou L, Yoshimura K, Kato T, Ohya K, Moriarty T, Emery K, Chen C-C, Gao J, Li G, Yang Y. Nat. Commun. 2013; 4:1446. [PubMed: 23385590]
24. Green MA, Emery K, Hishikawa Y, Warta W, Dunlop ED. Prog. Photovoltaics Res. Appl. 2013; 21:1–11.
25. Yue D, Khatav P, You F, Darling SB. Energy Environ. Sci. 2012; 5:9163–9172.
26. Lanzarini E, Antognazza MR, Biso M, Ansaldo A, Laudato L, Bruno P, Metrangolo P, Resnati G, Ricci D, Lanzani G. J. Phys. Chem. C. 2012; 116:10944–10949.
27. Esiner S, van Eersel H, Wienk MM, Janssen RAJ. Adv. Mater. 2013; 25:2932–2936.
28. Le Goff A, Artero V, Jousselme B, Tran PD, Guillet N, Metaye R, Fihri A, Palacin S, Fontecave M. Science. 2009; 326:1384–1387. [PubMed: 19965754]
29. Hinnemann B, Moses PG, Bonde J, Jørgensen KP, Nielsen JH, Horch S, Chorkendorff I, Nørskov JK. J. Am. Chem. Soc. 2005; 127:5308–5309. [PubMed: 15826154]
30. Nann T, Ibrahim SK, Woi P-M, Xu S, Ziegler J, Pickett CJ. Angew. Chem., Int. Ed. 2010; 49:1574–1577.
31. Sobczynski A. J. Catal. 1991; 131:156–166.
32. Jaramillo TF, Jørgensen KP, Bonde J, Nielsen JH, Horch S, Chorkendorff I. Science. 2007; 317:100–102. [PubMed: 17615351]
33. Laursen AB, Kegnaes S, Dahl S, Chorkendorff I. Energy Environ. Sci. 2011; 5:5577–5591.
34. Hou Y, Abrams BL, Vesborg PCK, Björketun ME, Herbst K, Bech L, Setti AM, Damsgaard CD, Pedersen T, Hansen O, Rossmeisl J, Dahl S, Nørskov JK, Chorkendorff I. Nat Mater. 2011; 10:434–438. [PubMed: 21516095]
35. Merki D, Fierro S, Vrubel H, Hu X. Chem. Sci. 2011; 2:1262–1267.
36. Merki D, Vrubel H, Hu X. Energy Environ. Sci. 2011; 2:1262–1267.
37. Tang ML, Grauer DC, Lassalle-Kaiser B, Yachandra VK, Amirav L, Long JR, Yano J, Alivisatos AP. Angew. Chem., Int. Ed. 2011; 50:10203–10207.
38. Wang T, Liu L, Zhu Z, Papakonstantinou P, Hu J, Liu H, Li M. Energy Environ. Sci. 2013; 6:625–633.
39. Thoi VS, Sun Y, Long JR, Chang CJ. Chem. Soc. Rev. 2012

40. Du P, Eisenberg R. Energy Environ. Sci. 2012; 5:6012–6021.
41. Tran PD, Artero V, Fontecave M. Energy Environ. Sci. 2010; 3:727–747.
42. Merki D, Hu X. Energy Environ. Sci. 2011; 4:3878–3888.
43. Schleich DM, Chang HS, Barberio YL, Hanson KJ. J. Electrochem. Soc. 1989; 136:3274–3278.
44. Ratnasamy P, Rodrique L, Leonard AJ. J. Phys. Chem. 1973; 77:2242–2245.
45. Hibble SJ, Wood GB. J. Am. Chem. Soc. 2003; 126:959–965. [PubMed: 14733573]
46. Müller A, Diemann E, Krickemeyer E, Walberg HJ, Bogge H, Armatage A. Eur. J. Solid State Inorg. Chem. 1993; 30:565–572.
47. Jiao H, Li Y-W, Delmon B, Halet J.-F. o. J. Am. Chem. Soc. 2001; 123:7334–7339. [PubMed: 11472162]
48. Andreasen B, Tanenbaum DM, Hermenau M, Voroshazi E, Lloyd MT, Galagan Y, Zimmernann B, Kudret S, Maes W, Lutsen L, Vanderzande D, Wurfel U, Andriessen R, Rosch R, Hoppe H, Teran-Escobar G, Lira-Cantu M, Rivaton A, Uzunoglu GY, Germack DS, Hosel M, Dam HF, Jorgensen M, Gevorgyan SA, Madsen MV, Bundgaard E, Krebs FC, Norrman K. Phys. Chem. Chem. Phys. 2012; 14:11780–11799. [PubMed: 22829118]
49. Nikiforov MP, Strzalka J, Darling SB. Sol. Energy Mater. Sol. Cells. 2013; 110:36–42.
50. Kim JY, Kim SH, Lee HH, Lee K, Ma W, Gong X, Heeger AJ. Adv. Mater. 2006; 18:572–576.
51. Kim JY, Lee K, Coates NE, Moses D, Nguyen TQ, Dante M, Heeger AJ. Science. 2007; 317:222–225. [PubMed: 17626879]
52. Lee K, Kim JY, Park SH, Kim SH, Cho S, Heeger AJ. Adv. Mater. 2007; 19:2445–2449.
53. Park SH, Roy A, Beaupre S, Cho S, Coates N, Moon JS, Moses D, Leclerc M, Lee K, Heeger AJ. Nat. Photonics. 2009; 3:297–302.
54. Fravventura MC, Deligiannis D, Schins JM, Siebbeles LDA, Savenije TJ. J. Phys. Chem. C. 2012; 117:8032–8040.
55. Dang MT, Hirsch L, Wantz G. Adv. Mater. 2011; 23:3597–3602. [PubMed: 21936074]
56. Boettcher SW, Warren EL, Putnam MC, Santori EA, Turner-Evans D, Kelzenberg MD, Walter MG, McKone JR, Brunschwig BS, Atwater HA, Lewis NS. J. Am. Chem. Soc. 2011; 133:1216–1219. [PubMed: 21214239]
57. McKone JR, Warren EL, Bierman MJ, Boettcher SW, Brunschwig BS, Lewis NS, Gray HB. Energy Environ. Sci. 2011; 4:3573–3583.
58. Seger B, Laursen AB, Vesborg PCK, Pedersen T, Hansen O, Dahl S, Chorkendorff I. Angew. Chem., Int. Ed. 2012; 51:9128–9131.
59. Tran PD, Pramana SS, Kale VS, Nguyen M, Chiam SY, Batabyal SK, Wong LH, Barber J, Loo J. Chem. - Eur. J. 2012; 18:13994–13999. [PubMed: 23008230]
60. Webster LR, Ibrahim SK, Wright JA, Pickett CJ. Chem. - Eur. J. 2012; 18:11798–11803. [PubMed: 22865600]
61. Paracchino A, Laporte V, Sivula K, Gratzel M, Thimsen E. Nat. Mater. 2011; 10:456–461. [PubMed: 21552270]
62. McKone JR, Pieterick AP, Gray HB, Lewis NS. J. Am. Chem. Soc. 2012; 135:223–231. [PubMed: 23198831]
63. Li L, Duan LL, Wen FY, Li C, Wang M, Hagfeld A, Sun LC. Chem. Com. 2012; 48:988–990.
64. Tong L, Iwase A, Nattestad A, Bach U, Weidelener M, Gotz G, Mishra A, Bauerle P, Amal R, Wallace GG, Mozer AJ. Energy Environ. Sci. 2012; 5:9472–9475.
65. Zong X, Na Y, Wen F, Ma G, Yang J, Wang D, Ma Y, Wang M, Sun L, Li C. Chem. Com. 2009:4536–4538.
66. Zong X, Yan H, Wu G, Ma G, Wen F, Wang L, Li C. J. Am. Chem. Soc. 2008; 130:7176–7177. [PubMed: 18473462]
67. Zong X, Wu G, Yan H, Ma G, Shi J, Wen F, Wang L, Li C. J. Phys. Chem. C. 2010; 114:1963–1968.
68. Frame FA, Osterloh FE. J. Phys. Chem. C. 2010; 114:10628–10633.
69. Merki D, Vrubel H, Rovelli L, Fierro S, Hu X. Chem. Sci. 2012; 3:2515–2525.

70. Tran PD, Nguyen M, Pramana SS, Bhattacharjee A, Chiam SY, Fize J, Field MJ, Artero V, Wong LH, Loo J, Barber J. Energy Environ. Sci. 2012; 5:8912–8916.

71. Tran PD, Le Goff A, Heidkamp J, Jousselme B, Guillet N, Palacin S, Dau H, Fontecave M, Artero V. Angew. Chem., Int. Ed. 2011; 50:1371–1374.

72. Andreiadis ES, Jacques P-A, Tran PD, Leyris A, Chavarot-Kerlidou M, Jousselme B, Matheron M, Pécaut J, Palacin S, Fontecave M, Artero V. Nat. Chem. 2013; 5:48–53. [PubMed: 23247177]

Europe PMC Funders Author Manuscripts

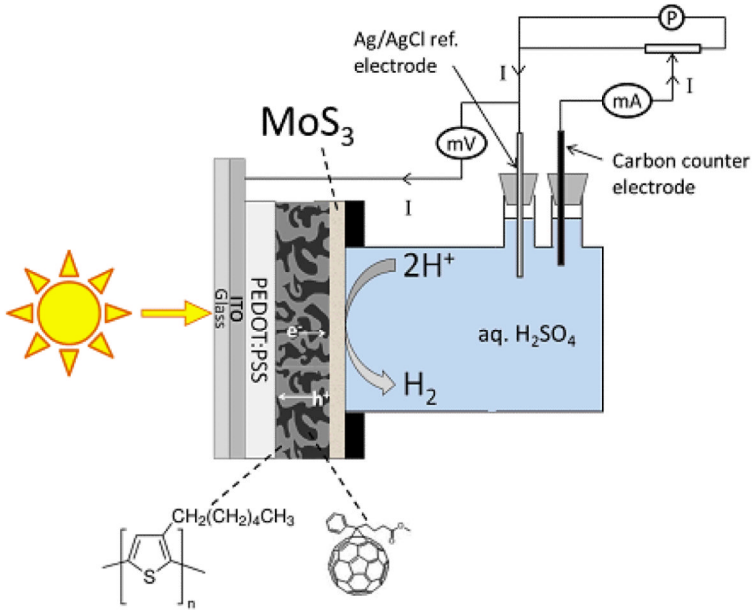

Fig. 1.

Architecture of the MoS_3/P3HT:PCBM H_2-evolving photocathode inserted in the cell used in this study for photo-electrochemical measurements.

Europe PMC Funders Author Manuscripts

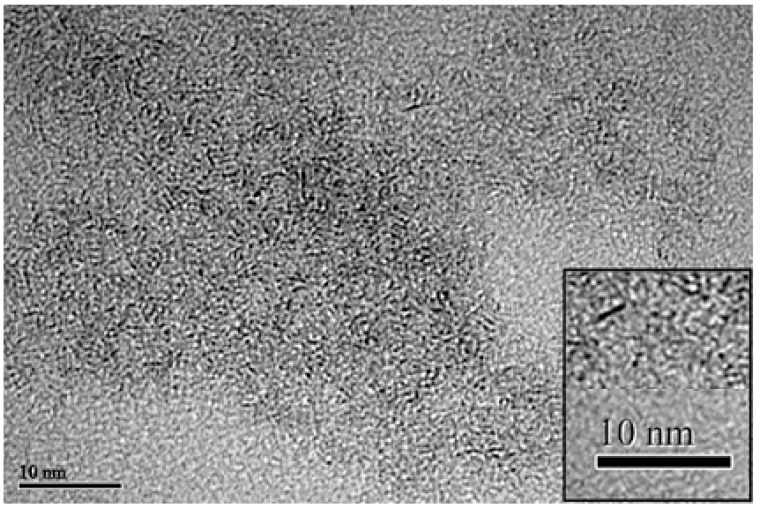

Fig. 2.
TEM analysis of precipitated MoS_3 nanoparticles (final pH was 2). Isolated particles and rods are clearly visible in the inset.

Europe PMC Funders Author Manuscripts

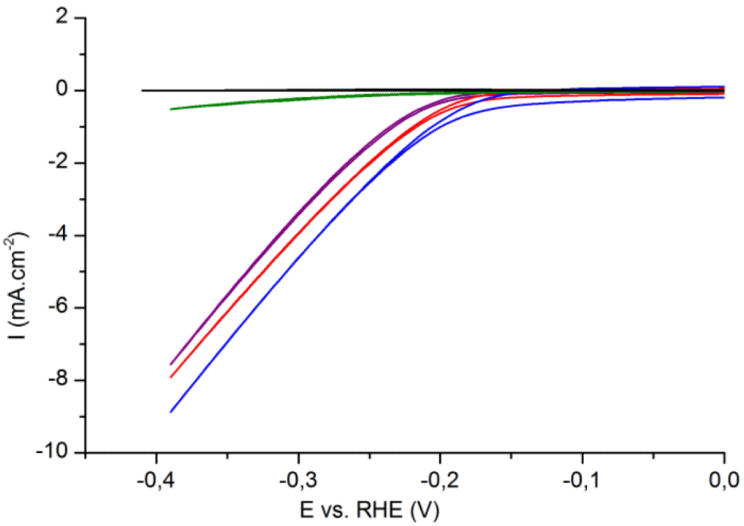

Fig. 3.

Cyclic voltammetry (50 $mV.s^{-1}$, third cycle shown) of an ITO-coated glass substrate (black) and of MoS_3 films deposited by spin coating on ITO-coated glass substrates, in H_2SO_4 0.5 M. Film thickness: 15nm (purple), 40nm (red), 90nm (blue), 200nm (green). Electrode surface area: 0.5 cm^2.

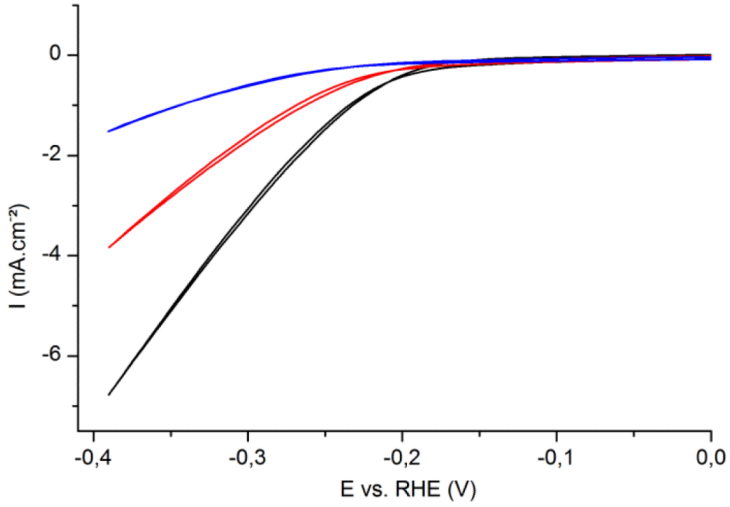

Fig. 4.

Cyclic voltammetry (50 $mV.s^{-1}$, third cycle shown) of MoS_3 films of different thicknesses deposited by spray on ITO-coated glass substrates, in H_2SO_4 0.5 M. Film thickness: 40 ± 20 nm (black), 100 ± 30 nm (red), 300 ± 100 nm (blue). Electrode surface area: 0.5 cm^2.

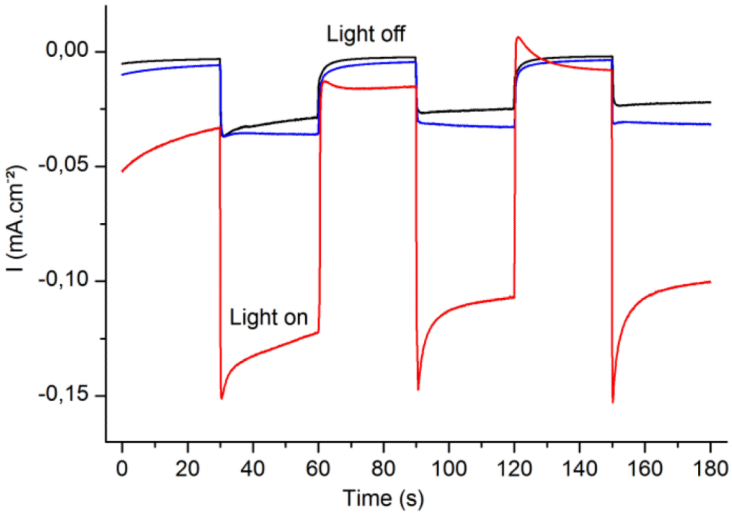

Fig. 5.

Caption Electrolysis at a bias potential of +0.16 V vs. RHE, with chopped visible light, in H_2SO_4 0.5 M. Black: P3HT:PCBM, blue: MoS_3 / P3HT:PCBM photocathode, red: TiO_2:MoS_3 / P3HT:PCBM photocathode. Electrode area: 0.5 cm^2.

Europe PMC Funders Author Manuscripts

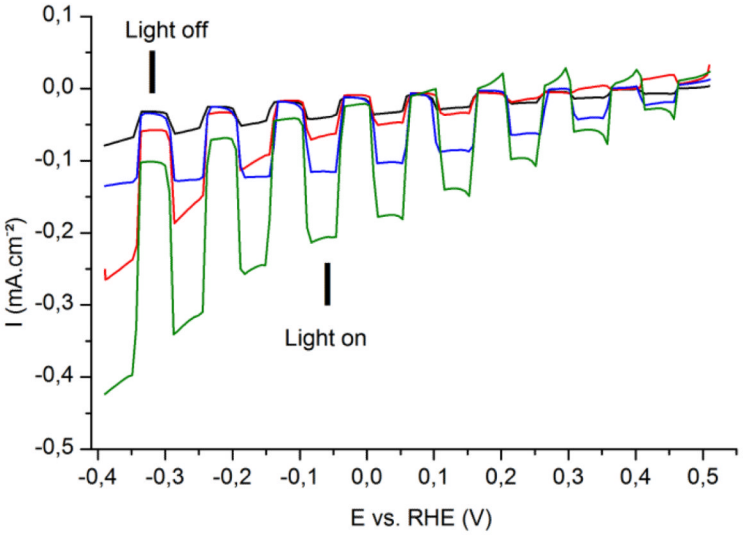

Fig. 6.

Linear sweep voltammograms recorded at 5 $mV.s^{-1}$ in H_2SO_4 0.5 M with chopped visible light for several photocathodes. Black: P3HT:PCBM (reference), red: MoS_3 / P3HT:PCBM photocathode, blue: TiO_2 / P3HT:PCBM photocathode, green: TiO_2:MoS_3 / P3HT:PCBM photocathode. Electrode area: 0.5 cm^2.

Europe PMC Funders Author Manuscripts